Proceedings of the Fifteenth International Conference on
Computational Structures Technology
Edited by: P. Iványi, J. Kruis and B.H.V. Topping
Civil-Comp Conferences, Volume 9, Paper 6.1
Civil-Comp Press, Edinburgh, United Kingdom, 2024
ISSN: 2753-3239, doi: 10.4203/ccc.9.6.1

A Stationary Streamline Integration Algorithm for Elastic-Plastic Bending of an Axially Moving Beam

J. Scheidl

Institute of Mechanics and Mechatronics, TU Wien, Vienna, Austria

Abstract

The efficient numerical treatment of the advection problem for the plastic variables is an important issue concerning the development of arbitrary Lagrangian Eulerian finite element schemes for the simulation of steady-state continuous metal forming processes. Structural finite elements for bending dominant applications such as sheet metal roll forming usually employ a kind of streamline integration procedure to address these advection problems. A novel scheme is devised as a modification of the corrector phase of a standard return-mapping algorithm that accomplishes a streamline integration in space for stationary processes. The algorithm is developed for an elastic-plastic bending problem of an axially moving beam and its capabalities are demonstrated in comparison to an established time stepping alternative.

Keywords: finite elements, metal plasticity, arbitrary Lagrangian Eulerian methods, axially moving continua, return-mapping algorithm, streamline integration

1 Introduction

The accurate and efficient simulation of continuous metal forming processes requires advanced numerical techniques. Here, a novel modification of the established elastic-

plastic return-mapping algorithm, see [1], is proposed, which has the potential to significantly accelerate simulations of steady-state bending dominant forming processes like sheet metal roll forming. In this academic study, a mixed Eulerian–Lagrangian beam finite element scheme, matched with a stress resultant plasticity model for pure elastic-plastic bending, is combined with the novel streamline integration algorithm for the advection of plastic variables; results are compared against an established transient time-stepping scheme.

Metal forming processes are difficult to simulate, owing to the fact that the material is moving across a control domain and deformed at spatially fixed forming stands, which impedes the applicability of standard Lagrangian (material) finite element models, see [2]. In response to these limitations different variants of the arbitrary Lagrangian Eulerian method (ALE) are developed that, based on some sort of coordinate transformation, allow for a resolution of the primary mechanical fields at fixed positions in transport direction, which effectively decouples the material transport from the deformation of the finite element mesh. In this regard, Eulerian–Lagrangian finite elements are used to simulate steady-state hot rolling in [3], ALE continuum finite elements featuring the full operator split method are applied to simulate roll forming of complex profiles in [4, 5] and a conceptually different mixed Eulerian–Lagrangian shell finite element model for roll forming is proposed in [6].

The mentioned decoupling of variables and material transport gives rise to advection problems owing to the transport of internal variables that are strictly attached to the particle motion. In the context of metal forming processes these internal variables characterise the plastic state of material particles and typically comprise plastic strains and hardening variables like the plastic dissipation work. Regardless of the chosen ALE implementation, the two distinguished strategies for the numerical solution of advection problems in steady-state forming processes are: the global resolution method and the streamline integration method, see [7]. The global resolution method applies a global weak formulation, typically using finite elements. It is applicable to models using unstructured meshes, but great care has to be taken in order to prevent spurious contributions to the states of individual particles due to "cross-wind diffusion" of surrounding areas. As its name implies, the streamline integration method aims to solve the advection problem along the individual particle trajectories. It is inherently free of "cross-wind diffusion" effects due to the independent numerical solution of the advection problem for each streamline. Naturally, it favours regular meshes with element edges and streamlines in proper alignment.

In the stationary state of contour motion, the particles of one dimensional, axially moving continua like beams, strings and rods are automatically aligned with their trajectories. Corresponding mixed Eulerian–Lagrangian finite element models for axially moving plates and shells exist as well, see [8, 9]. Thus, the streamline integration method is the natural choice for developing numerical schemes for continuous forming processes of thin structures. The variant employed for sheet metal roll forming in [6] relies on the established *streamline integration in time* (SIT), which features a transient time-stepping scheme that gradually approaches the sought-after steady-

state. In the following, we develop a time-saving alternative, correspondingly called *stationary streamline integration in space* (SIS), based on an exemplary study on the elastic-plastic bending of a moving Euler–Bernoulli beam. In an effort to arrive at an efficient self-contained structural model, a simple stress resultant plasticity model for pure beam bending is used, see [10, 11, 12] for related formulations and [13, 14] for the more common continuum-theory based approach with a thickness resolution of plastic variables. Numerical experiments demonstrate the capabilities of the novel SIS in comparison to the conventional SIT.

2 Eulerian–Lagrangian beam finite elements for steady-state elastic-plastic bending

To provide a proof of concept for the SIS procedure, we consider the problem of elastic-plastic bending of an axially moving beam. The reduced complexity of this test case allows for an effortless implementation of the respective finite element scheme in the commercial computer algebra system Wolfram Mathematica.

2.1 Problem statement and modelling remarks

The considered continuous elastic-plastic bending process for an initially straight Bernoulli-Euler beam is depicted in Figure 1. Since the fluxes of mass and energy

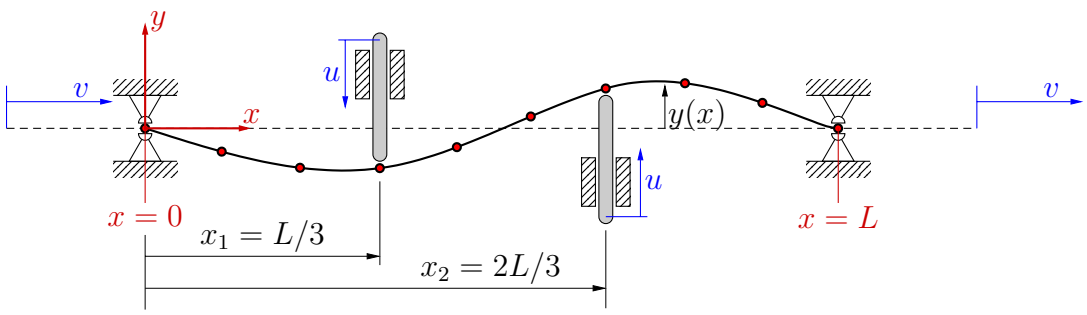

Figure 1: Steady-state elastic-plastic bending of an axially moving Euler–Bernoulli beam

across the domain boundaries are equilibrated at steady-state motion, it is sufficient to look at the active material volume currently residing in the open control domain $0 \leq x \leq L$, which is bounded by two rigid supports; the beam may rotate freely at the in- and outlet. Material particles enter and leave the domain at the constant transport rate v, which is assumed to be small enough that the problem can be considered quasistatic, i.e.: inertia effects are negligible.

Two pistons at the positions x_1 and x_2 induce bending and counter-bending of the beam by means of a kinematically prescribed displacement u; the contact interaction is assumed to be a frictionless point-contact for simplicity. The applied contact forces

F_1 and F_2, which amount to jumps in the transverse force at $\{x_1, x_2\}$, may be interpreted as the forming forces of the continuous bending operation. At small piston-deflections (small forming force levels) the beam will behave purely elastic; persistent plastic deformations, induced at higher load levels, are transported downstream with the given material transport rate; the constitutive relations of plasticity are discussed in Section 2.3.

The parameter set of the benchmark problem is provided in the SI-system of units: The beam has length $L = 1$ and is made of elastic ideal-plastic material with elastic modulus $E = 210 \times 10^9$ and yield strength $\sigma_f = 260 \times 10^6$. Its rectangular cross-section with width $H = 0.05$ and thickness $h = 0.01$ possesses the bending stiffness $a = EHh^3/12 = 875$. The two pistons are positioned at $x_1 = 1/3$ and $x_2 = 2/3$ and they are displaced simultaneously up to the maximum value $u_{\max} = 0.01$.

2.2 Kinematics of the stationary forming process

For a given load case the actual state is defined by the distribution of transverse deflections $y(x,t)$, the internal plastic variables $\boldsymbol{p}(x,t)$ and the set of material coordinates currently residing in the control domain $s = s(x,t)$:

$$s = x - vt, \quad s' = 1, \quad \dot{x} = v, \tag{1}$$

where the usual prime / dot notation is used to designate spatial derivatives and material (total) time derivatives, respectively. Note that derivatives with respect to the material arc coordinate s and the spatial coordinate x are interchangeable in the framework of the geometrically linear theory. The material time derivatives of the primary variables read:

$$\dot{y} = y'v + \partial_t y, \quad \dot{\boldsymbol{p}} = \boldsymbol{p}'v + \partial_t \boldsymbol{p}, \tag{2}$$

where the abbreviation ∂_t denotes local time derivatives at axially fixed points, i.e.: $\partial_t\{y, \boldsymbol{p}\} = \partial\{y, \boldsymbol{p}\}/\partial t|_{x=\text{const}}$. The Eulerian parametrisation in the spatial coordinate x (instead of the Lagrangian s) facilitates the enforcement of spatially-fixed boundary conditions for the moving system. Moreover, it allows for an easy identification of a stationary state by means of a time-independence of primary variables, which is synonymous with the self-equilibration of material and convective derivatives:

$$\partial_t y = \dot{y} - y'v = 0, \quad \partial_t \boldsymbol{p} = \dot{\boldsymbol{p}} - \boldsymbol{p}'v = 0. \tag{3}$$

Hence, the stationary state is a kind of contour-motion, where the material particles travel with constant rate v through a statically deflected configuration $y = y(x)$, while sustaining persistent plastic deformations due to $\boldsymbol{p} = \boldsymbol{p}(x)$ along the way. The two simulation strategies to compute this practically important steady-state, essentially differ in the enforcement of the constraint $\partial_t \boldsymbol{p} = 0$, see Section 2.5 and Section 2.6.

2.3 Stress resultant plasticity for pure beam bending

Plasticity is treated with a basic stress resultant plasticity model designed for pure elastic-plastic bending of a beam made of elastic ideal-plastic material. Thus, it cap-

tures the most important deformation mechanism for bending dominant forming processes. In contrast to the established approach to treat the material laws on the continuum level, there is no need for a resolution of plastic states in thickness direction as the constitutive relations are formulated on the structural level of the one-dimensional beam. Consequently, the stress resultant model is numerically efficient, but limited in terms of practical applicability, see [6, 12] for related models in the context of sheet metal roll forming.

As in classic continuum plasticity theory, see [15], the governing equations of the stress resultant plasticity model comprise: a yield criterion, an associated flow rule and a set of hardening rules to match the number of internal hardening variables. The stress resultant in the cross-section to distinguish elastic from elastic-plastic states for the pure bending case of an Euler–Bernoulli beam is the bending moment. Hence, the yield criterion merely needs to compare the actual bending moment M to the current yield moment M_f that indicates yielding:

$$F = \left(M^2 - M_f(A_p)^2\right) \leq 0, \tag{4}$$

where $F < 0$ designates elastic and $F = 0$ elastic-plastic states; squaring of the terms takes care of negative bending moments. The plastic work per unit length A_p governs the evolution of the yield moment M_f as the plastification of the cross-section progresses. The work conjugate of the bending moment is the curvature κ, which in the spirit of the additive decomposition of small strains in continuum theory is split in elastic and plastic parts:

$$\kappa = \kappa_e + \kappa_p, \tag{5}$$

where only the elastic material curvature κ_e enters the constitutive relation with bending stiffness a:

$$M = a\kappa_e = a(\kappa - \kappa_p). \tag{6}$$

The associated flow rule for the plastic strains κ_p and the evolution laws for the internal variable A_p read:

$$\dot{\kappa}_p = \dot{\lambda}\frac{\partial F}{\partial M}, \quad \dot{A}_p = M\dot{\kappa}_p, \tag{7}$$

with the non-negative increment of the consistency factor $\dot{\lambda}$. Evidently, the associated flow rule ensures that the plastic dissipation power stays positive at all times: $\dot{A}_p = 2\dot{\lambda}M^2 \geq 0$. The requirement that elastic-plastic states must reside on the current yield surface amounts to a constraint for $\dot{\lambda}$. In the context of incremental numerical schemes, see [16], this condition is either enforced by $F = 0$ directly or by demanding a respective alignment of the plastic flow with $\dot{F} = 0$, which is usually referred to as consistency condition:

$$\dot{F} = 2M\dot{M} - 2M_f(A_p)M_f'(A_p)\dot{A}_p = 0. \tag{8}$$

Making use of (5)–(7) we obtain a version that expresses $\dot{\lambda}$ in terms of the total curvature strain increments $\dot{\kappa}$:

$$\dot{\lambda} = \frac{a}{2M\left(a + M_f(A_p)M_f'(A_p)\right)}\dot{\kappa}. \tag{9}$$

Equations (7) and (9) form a closed set of plastic evolution laws that can be conveniently addressed with standard return-mapping algorithms, see [1].

It remains to state the aforementioned hardening rule that governs the evolution of the yield moment $M_f = M_f(A_p)$, which is illustrated in Figure 2. It is important

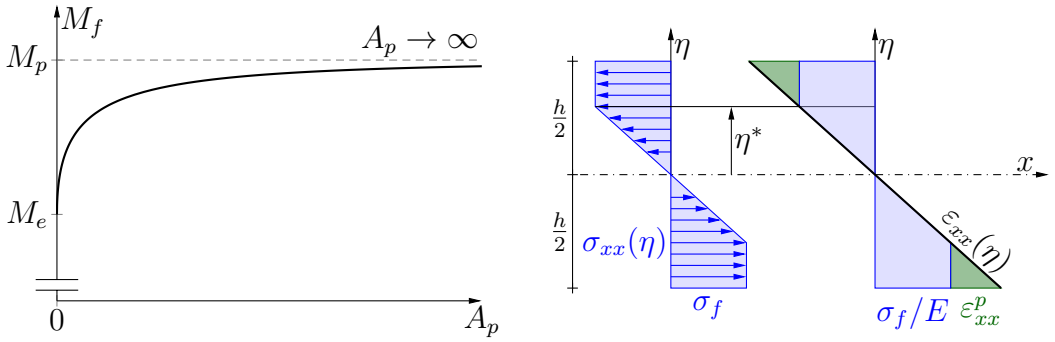

Figure 2: Pure elastic-plastic bending of a rectangular cross-section made of elastic ideal-plastic material; the yield moment M_f exhibits a kind of isotropic work hardening behaviour as plastification progresses for monotonically increasing loading.

to note, that this kind of "structural hardening" due to the progressing cross-section plastification appears independent of material hardening. Both structural and isotropic material hardening effects may be conveniently combined in terms of enhanced work hardening laws that include additional internal variables to govern the material hardening behaviour, see [12]. Here, we formulate this structural hardening law explicitly in its simplest form for the case of pure bending of an elastic-ideal plastic material. The derivation is easy to retrace following the annotations provided in Figure 2, see also [15]. The individual steps comprise: application of the Bernoulli-Euler kinematic hypothesis to the continuum body, which yields an inner elastic and an outer elastic-plastic region; the boundary η^* marks the transition between the two regions. The axial stresses $\sigma_{xx}(\eta)$ vary linearly in the inner region ($|\eta| < \eta^*$) and equal the constant yield stress σ_f in the outer region ($|\eta| \geq \eta^*$). The axial plastic strains are obtained from the additive decomposition of the strain state $\varepsilon_{xx} = \varepsilon^e_{xx} + \varepsilon^p_{xx}$. This enables computation of the yield moment M_f and the plastic dissipation work A_p as functions of the elastic-plastic boundary η^* by means of integrals over the thickness coordinate η. Finally, the structural hardening rule is obtained by substitution of the inverted formula $\eta^* = \eta^*(A_p)$ in the expression for the yield moment:

$$M_f(A_p) = \frac{H\sigma_f}{12}\left(3h^2 - \frac{\left(EA_p + hH\sigma_f^2 - \sqrt{EA_p\left(EA_p + 2hH\sigma_f^2\right)}\right)^2}{H^2\sigma_f^4}\right). \quad (10)$$

Observe that the elastic limit $M_f(0) = M_e = \sigma_f Hh^2/6$ equals two thirds of the plastic limit load $\lim_{A_p\to\infty} M_f(A_p) = M_p = \sigma_f Hh^2/4$.

2.4 Finite element implementation

We employ linear beam finite elements to approximately solve the continuous elastic-plastic beam bending process. Equilibrium states in the quasistatic framework are identified by a minimum of the total potential energy, which, owing to the kinematic type of loading, equals the strain energy:

$$U = \int_0^L \frac{1}{2} a \left(y'' - \kappa_p\right)^2 \, \mathrm{d}x. \tag{11}$$

Here, the material curvature κ has already been replaced with the second derivative of the transverse displacements y'' in accordance with the linear theory. The stationary state is characterised by a time-independent equilibrium distribution of transverse deflections $y(x)$ and plastic variables $\boldsymbol{p}(x)$, which comprise the plastic curvature κ_p, the plastic dissipation A_p and the consistency factor λ.

For a given load case, as defined by the piston displacement u, the final stationary state is computed by means of a homotopy procedure with increments of the piston displacement Δu. A proper algorithm to compute intermediate solutions for a single increment Δu has to:

- accomplish convergence to a both statically and plastically admissible state that satisfies the mechanical equilibrium and nowhere contradicts the yield criterion (4),
- consistently account for the transport of plastic variables with the material transport rate v.

Two capable strategies are the standard streamline integration in time (SIT), recapitulated in Section 2.5, and the stationary streamline integration in space (SIS), introduced in Section 2.5. Both emanate from the iterative return-mapping algorithm traditionally used for static problems, but essentially differ in the way the advection problem of plastic variables is addressed.

The displacement based finite element scheme, see [17], features a smooth approximation of transverse displacements $y(\xi, t)$ and a discrete resolution of plastic variables $\boldsymbol{p}$ at the finite element integration points. The ansatz features a cubic interpolation of the nodal displacements y_i and the derivatives $(\partial_\xi y)_i$ with respect to the normalised finite element coordinate $-1 \leq \xi \leq 1$:

$$y(\xi, t) = y_i(t)\, \psi_1(\xi) + (\partial_\xi y)_i(t)\, \psi_2(\xi) + y_{i+1}(t)\, \psi_3(\xi) + (\partial_\xi y)_{i+1}(t)\, \psi_4(\xi), \tag{12}$$

where i ist the nodal index and ψ_j denotes the usual Hermitian polynomials, depicted in Figure 3. These shape functions are constructed in correspondence with their designated nodal degrees of freedom; for example: $\psi_1(-1) = 1$, but $\partial_\xi \psi_1(-1) = \psi_1(1) = \partial_\xi \psi_1(1) = 0$. For equidistant meshes with constant element length $\Delta x = L/n$, where n is the total number of elements in the model, a linear interpolation of the axial coordinate $x(\xi)$ suffices to ensure a C^1-continuous approximation that is required by the

unshearable theory. With the element index $k \in [1, n]$, the linear interpolation for the k-th element reads:

$$x_k(\xi) = k\Delta x + \frac{\Delta x}{2}(\xi - 1). \tag{13}$$

The strain energy of the complete model is assembled as a sum of individual finite element contributions:

$$U = \sum_{k=1}^{n} \int_{-1}^{1} \frac{1}{2} a \left(y'' - \kappa_p\right)^2 \partial_\xi x \, \mathrm{d}\xi. \tag{14}$$

As indicated in Figure 3, the above normalised integrals are evaluated numerically using a three-point Gaussian quadrature rule, which is why the discrete resolution of the plastic variables at these integration points is sufficient.

2.5 Streamline integration in time (SIT)

This procedure is an established scheme to solve advection problems that naturally arise in arbitrary Lagrangian Eulerian formulations for the simulation of continuous metal forming processes. The idea is to fully separate the equilibrium iterations and the transport of plastic variables in a two stage process:

1. First a standard return-mapping scheme, see [1], is employed to iteratively compute a both statically and plastically admissible equilibrium state. In the predictor phase, an elastic mechanical equilibrium is predicted seeking a minimum of the total potential energy (11) under the assumption that the plastic variables $\boldsymbol{p}$ remain unchanged. Due to the linearity of the equilibrium equations for the Euler–Bernoulli beam model, the elastic predictor is obtained in a single step. In the corrector phase, the predicted state is used to update the plastic variables, wherever the elastic predictor exceeds the yield surface (4). The elastic-plastic evolution laws (7) and the consistency condition (9) are evaluated to arrive at a plastically admissible state. Elastic predictor and plastic corrector are alternated in a fixed point iteration that gradually approaches a both statically and plastically admissible equilibrium.

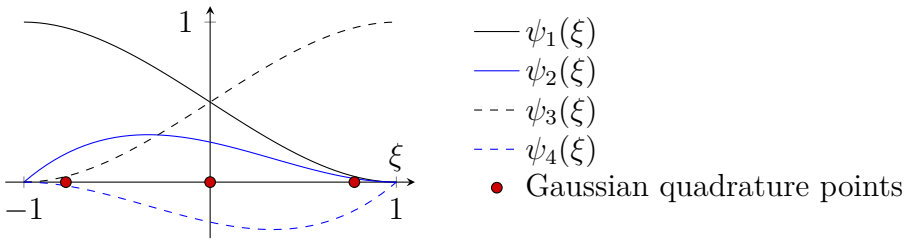

Figure 3: Hermitian polynomials and three-point Gaussian quadrature points for the finite element approximation

2. Secondly, the converged plastic states as obtained from the first stage are transported in axial direction by means of a forward in time backwards in space finite difference scheme. The plastic states at the individual material particles are kept constant during the advection, which essentially perturbs the previously obtained equilibrium. In this respect, the transport of plastic variables may be viewed as a load increment of the time stepping scheme.

As stages 1 and 2 are alternated in the outer loop, the transient time stepping solution gradually approaches the stationary state, which in terms of the plastic variables according to (3) is characterised by:

$$\partial_t \boldsymbol{p} = \dot{\boldsymbol{p}} - \boldsymbol{p}' v = 0. \tag{15}$$

The operation principle of the SIT in the finite element framework is best interpreted with respect to this formula: First, the predictor-corrector stage yields material increments of the plastic variables at all integration points $\dot{\boldsymbol{p}}(x_\alpha, t)$, which are situated at the positions x_α; α is the global integration point index with $1 \leq \alpha \leq 3n$ due to the three-point quadrature rule. The material plastic increments are held constant during the second stage that invokes the forward in time backwards in space finite different scheme to account for the transport of material particles:

$$\boldsymbol{p}(x_\alpha, t + \Delta t) = \boldsymbol{p}(x_\alpha, t) + \dot{\boldsymbol{p}}(x_\alpha, t)\, \Delta t - \frac{\boldsymbol{p}(x_\alpha, t) - \boldsymbol{p}(x_{\alpha-1}, t)}{x_\alpha - x_{\alpha-1}} v\, \Delta t \tag{16}$$

Convergence to the stationary state may be judged after completion of the second stage by comparison of $\boldsymbol{p}(x_\alpha, t + \Delta t)$ against the values of the previous step. The backward finite difference for $\boldsymbol{p}'$ ensures stability of the numerical scheme; using an explicit formula as done in (16) facilitates a sequential solution of the problem. Note that this transient time integration approach depends on the choice of the numerical parameters Δt and v. This also implies a mesh dependence of the advection scheme (16) owing to the fact that the material displacement increment $v\Delta t$ should not surpass the minimum integration point distance, i.e.: $v\Delta t < \min\left(x_\alpha - x_{\alpha-1}\right)$ for all $\alpha > 1$.

2.6 Stationary streamline integration in space (SIS)

The SIS employs a modified predictor-corrector scheme that incorporates the advection problem into the corrector phase of the return-mapping algorithm. For this sake, the condition of stationary operation for the plastic variables (3) is enforced directly by means of:

$$\dot{\boldsymbol{p}} = v \boldsymbol{p}', \tag{17}$$

which allows to rewrite the evolution laws of plasticity (7) in terms of derivatives with respect to the spatial coordinate x:

$$\kappa_p' = \lambda' \frac{\partial F}{\partial M} = 2M\lambda', \quad A_p' = M{\kappa'}_p = 2M^2\lambda'. \tag{18}$$

With the elastic predictor computed from the equilibrium equations in the usual fashion, these equations constitute initial value problems in space that can be discretised using finite differences:

$$\begin{aligned} \kappa_p(x_\alpha) &= \kappa_p(x_{\alpha-1}) + 2M\,(\lambda(x_\alpha) - \lambda(x_{\alpha-1})) \\ A_p(x_\alpha) &= A_p(x_{\alpha-1}) + 2M^2\,(\lambda(x_\alpha) - \lambda(x_{\alpha-1})). \end{aligned} \tag{19}$$

The scheme is backwards in space and fully implicit. The finite difference grid sizes on both sides cancel each other out and, once again, the coordinates x_α indicate integration point positions. Observe that the performed time-to-space transformation of derivatives has fully eliminated the dependence on time t and transport velocity v.

With the consitutive relation for the bending moment (6) at hand, the finite difference relations (19) determine the actual states of the plastic curvature and dissipation work at the next integration point downstream, once the consistency factor $\lambda(x_\alpha)$ is computed numerically from the root problem $F = 0$, which directly enforces the yield condition (4). Alternatively, a combined finite difference integration with the additional consistency condition (9) reformulated for λ' in the same fashion can be performed. However, judging by the numerical experiments conducted for the present beam model, the above root-finding variant appears to work more reliably.

The final numerical simulation for a given load case is obtained through stepwise increasing the piston displacement with constant steps Δu up to the desired value $u_{\max}$. The fixed point iteration for a single load increment features an alternation of the usual elastic predictor and the just described SIS, which provides a "stationary" plastic corrector for the next iteration. In contrast to the previously discussed SIT, the SIS estimate of the stationary equilibrium gradually improves with each step, which should significantly speed up equilibrium iterations in nonlinear problems. Another major benefit of the SIS lies in its capability to perform parameter studies very efficiently, since every single equilibrium state obtained for a given load increment Δu is itself a stationary state that possesses practical relevance.

3 Results of the benchmark study

Corresponding finite element solutions for the benchmark problem with parameters according to Section 2.1 are computed for both algorithms. As the sole source of loading, the piston displacement is incrementally increased from the initial value $u_0 = 0.0044$, which is very close to the limit of first yield, up to the final value $u_{\max} = 0.01$. For the SIS algorithm a total of 28 steps of magnitude $\Delta u = 0.0002$ is performed; 20 predictor-corrector fixed point iterations are conducted for each step to ensure convergence to the respective steady-state. Load incrementation by means of Δu and time-stepping with step $\Delta t = 0.01$ and transport rate $v = 0.5$ are combined in a single homotopy scheme for the SIT. A total of 600 time steps with 10 predictor-corrector iterations each are undertaken. The piston incrementation is finished after one second of the total simulation time $t_{\text{total}} = 3$, afterwards the transient

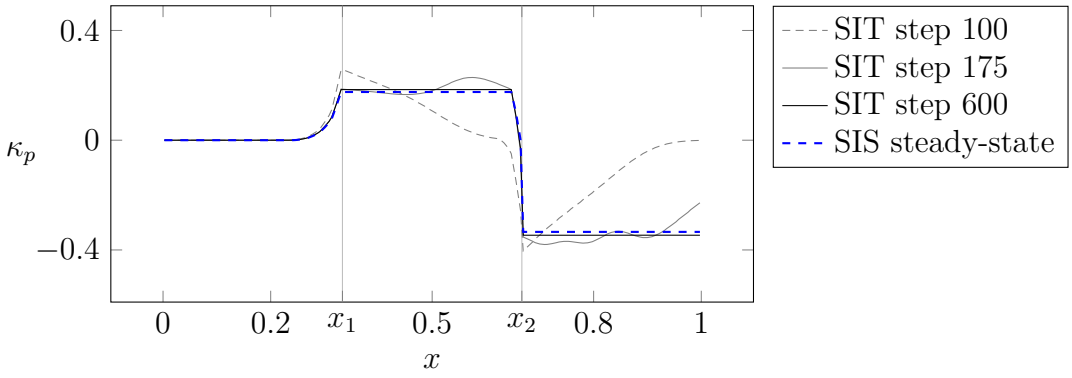

Figure 4: Gradual convergence of the transient SIT time-stepping procedure towards the stationary SIS solution in terms of the distribution of the plastic curvature κ_p.

solution gradually converges towards the steady-state. Simulations are conducted in the Wolfram Mathematica environment on an Intel(R) Xeon(R) CPU E5-2640 v3 at 2.60GHz.

A collection of characteristic results, including the computation timings given in seconds, for equidistant meshes with 15, 30 and 45 finite elements is presented in Table 1. Though the numerical parameters have not been optimised for maximum

	timings [s]		$\kappa_p(x=L)$		F_1		F_2	
n	SIS	SIT	SIS	SIT	SIS	SIT	SIS	SIT
15	64	982	-0.321	-0.3378	2745	2753	2786	2786
30	206	2961	-0.3349	-0.3473	2705	2698	2781	2690
45	480	6734	-0.3342	-0.3464	2692	2675	2794	2415

Table 1: Comparison of timings and selected results for computations with SIT and SIS algorithms.

efficiency, the great time saving potential of the SIS algorithm is evident. The increasing discrepancy for the forming forces at finer discretisation levels arises due to the coarseness of the constant time-step in relation to the mesh size that affects the accuracy of the finite difference integration (16). Evidently, the SIT requires correspondingly smaller time steps for refined meshes. Apart from that, the results for forming forces and resultant plastic curvature demonstrate correspondence of the two solution schemes which is further substantiated by the graphical overlay of solutions for the plastic curvature κ_p in Figure 4. The plots at different simulation times for the SIT simulation visualise the slowly evolving congruence to the steady-state solution of the SIS scheme. Note that the counter bending at the second piston induces a sign change of κ_p and thus reverse plasticity, which is a phenomenon that cannot be captured accurately by the employed pure bending stress resultant plasticity model.

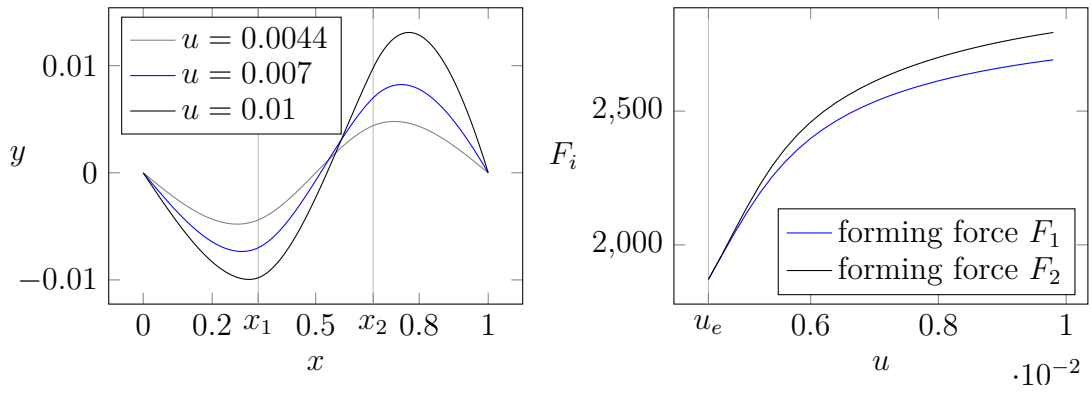

Figure 5: Steady state beam transverse deflections (left) and evolution of forming forces at both pistons (right) for increasing piston displacements u.

Though insignificant for the present academic study, this observation indicates that the beam bending problem provides an opportunity for the numerical verification of advanced stress resultant plasticity models that include kinematic hardening.

Finally, Figure 5 depicts three stationary configurations as well as the evolution of the forming forces for increasing piston displacement u. It illustrates the aptitude of the SIS algorithm for parameter studies, which is attributed to the fact that the solution path traces a sequence of stationary states. The horizontal shifting of the local peaks of the transverse deflection y is a consequence of the axial motion of the beam. The graphs for the forming forces originate from the elastic boundary; their degressive nature relates to the progressing plastification, which results in a softening behaviour of the structure.

4 Concluding remarks

The proposed stationary streamline integration in space (SIS) constitutes a novel algorithmic approach for the arbitrary Lagrangian Eulerian finite element simulation of steady-state forming processes of thin structures. Other stationary solution algorithms available in the literature are designed for classic rolling applications that necessitate a continuum-based treatment, see [7]. The here presented SIS implementation aims for bending dominant forming processes that may be approached with structural models of beams, plates or shells. In this respect the combination of structural theory with a proper stress resultant plasticity model and the novel SIS scheme possesses great potential for the efficient simulation of bending dominant processes.

In contrast to the established streamline integration in time (SIT), where equilibrium iterations and convective transport are treated separately, the SIS integrates the advection problem in the corrector step of the elastic-plastic return-mapping algorithm. As explained earlier and partially demonstrated by the exemplary numerical study the major advantages of this strategy comprise:

- a significant reduction of simulation times: For the considered beam benchmark problem, time savings amount to over $90\,\%$.
- the capability to perform efficient parameter studies, as the incremental solution up to a final steady-state via some kind homotopy strategy follows a path of stationary states.
- the independence of numerical time stepping parameters and the mesh-independence of the finite difference scheme used to integrate the initial value problem during the corrector phase of the stationary scheme.
- the automatic acceleration of equilibrium iterations during the predictor step as the iterative scheme approaches a stationary state; additional measures are necessary to reach a similar behaviour for the SIT, see [18].

In future, the ongoing development of the SIS shall primarily focus on augmentations of the simulation model towards a more realistic model of a continuous bending dominant process such as sheet metal roll forming. Important extensions in this regard comprise: the account for large geometrically nonlinear deformations, the implementation in mixed finite element models of plates and shells, the introduction of solid body distributed contact with actual forming tools (potentially including friction) as well as the implementation of more complicated plasticity models, such as the stress resultant plasticity model proposed in [19]. These extensions will likely necessitate adaptions that shall contribute to the continued improvement of the present SIS algorithm towards a more evolved scheme.

References

[1] JC Simo and RL Taylor. A return mapping algorithm for plane stress elastoplasticity. *International Journal for Numerical Methods in Engineering*, 22(3): 649–670, 1986.

[2] Ivo Steinbrecher, Alexander Humer, and Loc Vu-Quoc. On the numerical modeling of sliding beams: A comparison of different approaches. *Journal of Sound and Vibration*, 408:270–290, 2017. ISSN 0022-460X. doi: https://doi.org/10.1016/j.jsv.2017.07.010.

[3] Josef Synka, Alexander Kainz, Robert Maringer, and Andreas Obereder. Numerical analysis of a new eulerian–lagrangian finite element method applied to steady-state hot rolling processes. *International Journal for Numerical Methods in Engineering*, 62(5):616–638, 2005. doi: https://doi.org/10.1002/nme.1183.

[4] R. Boman, L. Papeleux, Q.V. Bui, and J.P. Ponthot. Application of the arbitrary lagrangian eulerian formulation to the numerical simulation of cold roll forming process. *Journal of Materials Processing Technology*, 177(1):621–625,

2006. ISSN 0924-0136. doi: https://doi.org/10.1016/j.jmatprotec.2006.04.120. Proceedings of the 11th International Conference on Metal Forming 2006.

[5] Yanick Crutzen, Romain Boman, Luc Papeleux, and Jean-Philippe Ponthot. Lagrangian and arbitrary lagrangian eulerian simulations of complex roll-forming processes. *Comptes Rendus Mécanique*, 344(4):251–266, 2016. ISSN 1631-0721. doi: https://doi.org/10.1016/j.crme.2016.02.005. Computational simulation of manufacturing processes.

[6] Emin Kocbay, Jakob Scheidl, Fabian Riegler, Martin Leonhartsberger, Matthias Lamprecht, and Yury Vetyukov. Mixed eulerian–lagrangian modeling of sheet metal roll forming. *Thin-Walled Structures*, 186:110662, 2023. ISSN 0263-8231. doi: https://doi.org/10.1016/j.tws.2023.110662.

[7] Shitij Arora. *Steady-state formulation of metal forming processes : Contact coupling and treatment of history-dependent material models with unstructured meshes*. Theses, Université Paris sciences et lettres, November 2020. URL `https://pastel.hal.science/tel-04099109`.

[8] Yu. Vetyukov, P. G. Gruber, and M. Krommer. Nonlinear model of an axially moving plate in a mixed Eulerian–Lagrangian framework. *Acta Mechanica*, 227 (10):2831–2842, 2016. ISSN 1619-6937. doi: 10.1007/s00707-016-1651-0.

[9] Jakob Scheidl, Yury Vetyukov, Christian Schmidrathner, Klemens Schulmeister, and Michael Proschek. Mixed Eulerian–Lagrangian shell model for lateral run-off in a steel belt drive and its experimental validation. *International Journal of Mechanical Sciences*, 204:106572, 2021. ISSN 0020-7403. doi: https://doi.org/10.1016/j.ijmecsci.2021.106572.

[10] Juan Carlos Simo and J G Kennedy. On a stress resultant geometrically exact shell model. Part V. Nonlinear plasticity: formulation and integration algorithms. *Computer Methods in Applied Mechanics and Engineering*, 96(2): 133–171, 1992.

[11] Jaka Dujc and Boštjan Brank. On stress resultant plasticity and viscoplasticity for metal plates. *Finite Elements in Analysis and Design*, 44(4):174–185, 2008. ISSN 0168-874X. doi: https://doi.org/10.1016/j.finel.2007.11.011.

[12] Emin Kocbay and Yury Vetyukov. Stress resultant plasticity for plate bending in the context of roll forming of sheet metal. *International Journal for Numerical Methods in Engineering*, 122(18):5144–5168, 2021. doi: https://doi.org/10.1002/nme.6760.

[13] Q.V. Bui and J.P. Ponthot. Numerical simulation of cold roll-forming processes. *Journal of Materials Processing Technology*, 202(1):275–282, 2008. ISSN 0924-0136. doi: https://doi.org/10.1016/j.jmatprotec.2007.08.073.

[14] M.D. Alaydin, D.J. Benson, and Y. Bazilevs. An updated lagrangian framework for isogeometric kirchhoff–love thin-shell analysis. *Computer Methods in Applied Mechanics and Engineering*, 384:113977, 2021. ISSN 0045-7825. doi: https://doi.org/10.1016/j.cma.2021.113977.

[15] Jacob Lubliner. *Plasticity theory*. Dover Publications, Inc., 2008. ISBN 9780486462905.

[16] D. R. J. Owen E. A. de Souza Neto, D. Perić. *Computational Methods for Plasticity*. John Wiley & Sons, Ltd, 2008. ISBN 9780470694626. doi: https://doi.org/10.1002/9780470694626.

[17] Yury Vetyukov. *Nonlinear Mechanics of Thin-Walled Structures: Asymptotics, Direct Approach and Numerical Analysis*. Springer Vienna, Vienna, 2014. ISBN 978-3-7091-1777-4. doi: 10.1007/978-3-7091-1777-4.

[18] H.H. Wisselink and J. Huétink. 3d fem simulation of stationary metal forming processes with applications to slitting and rolling. *Journal of Materials Processing Technology*, 148(3):328–341, 2004. ISSN 0924-0136. doi: https://doi.org/10.1016/j.jmatprotec.2004.02.036.

[19] Emin Kocbay, Jakob Scheidl, Fabian Schwarzinger, and Yury Vetyukov. An enhanced stress resultant plasticity model for shell structures with application in sheet metal roll forming. *The International Journal of Advanced Manufacturing Technology*, 130(1):781–798, Jan 2024. ISSN 1433-3015. doi: 10.1007/s00170-023-12544-1.